The Abdus Salam
International Centre for Theoretical Physics

United Nations
Educational, Scientific and
Cultural Organization

IAEA

2168-14

Joint ICTP-IAEA Workshop on Dense Magnetized Plasma and Plasma Diagnostics

15 - 26 November 2010

Introduction to Spectroscopy

H-J. Kunze

Ruhr Universitat Bochum
Bochum
Germany

Introduction to Plasma Spectroscopic Techniques

H.-J. Kunze

Institute for Experimental Physics V, Ruhr-University,
44780 Bochum, Germany

Joint ICTP/IAEA Workshop on Dense Magnetized Plasma
and Plasma Diagnostics, Trieste, 15-26 November 2010

Typical Spectrum

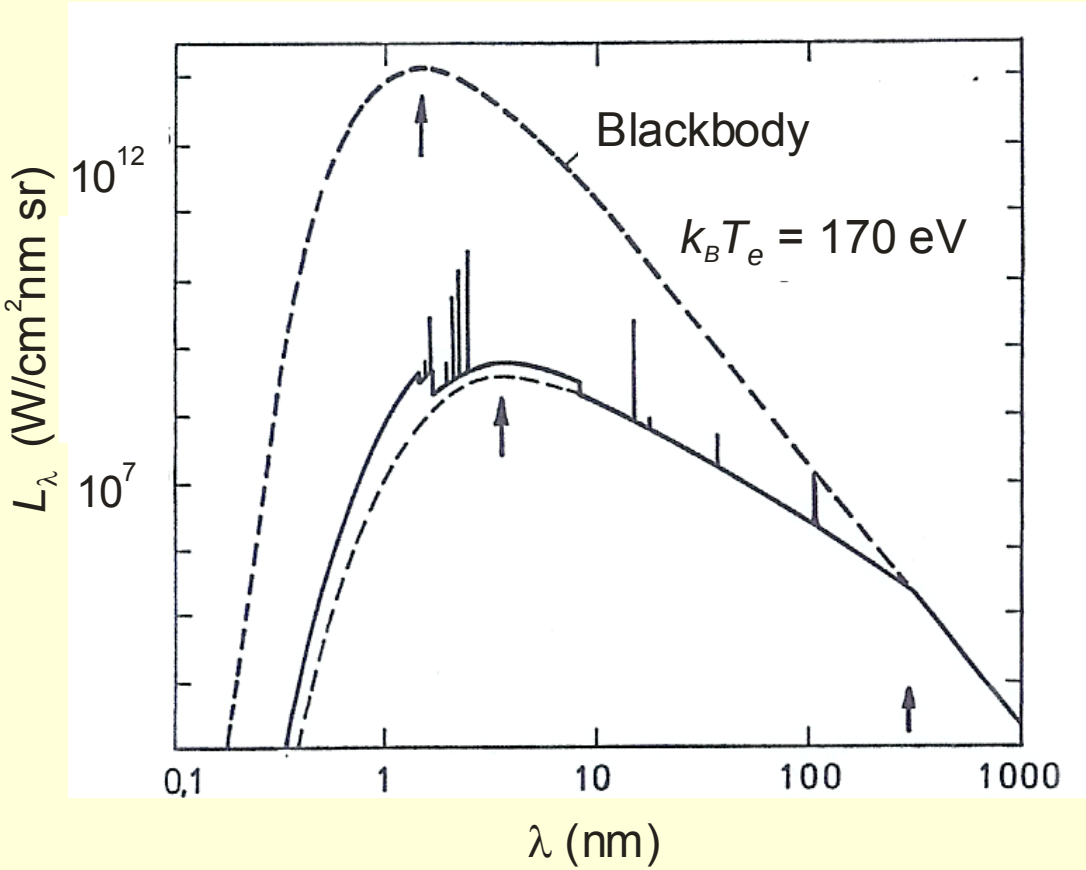

Continuum radiation

bremsstrahlung free-free transitions

recombination radiation free-bound transitions

Line radiation bound-bound transitions

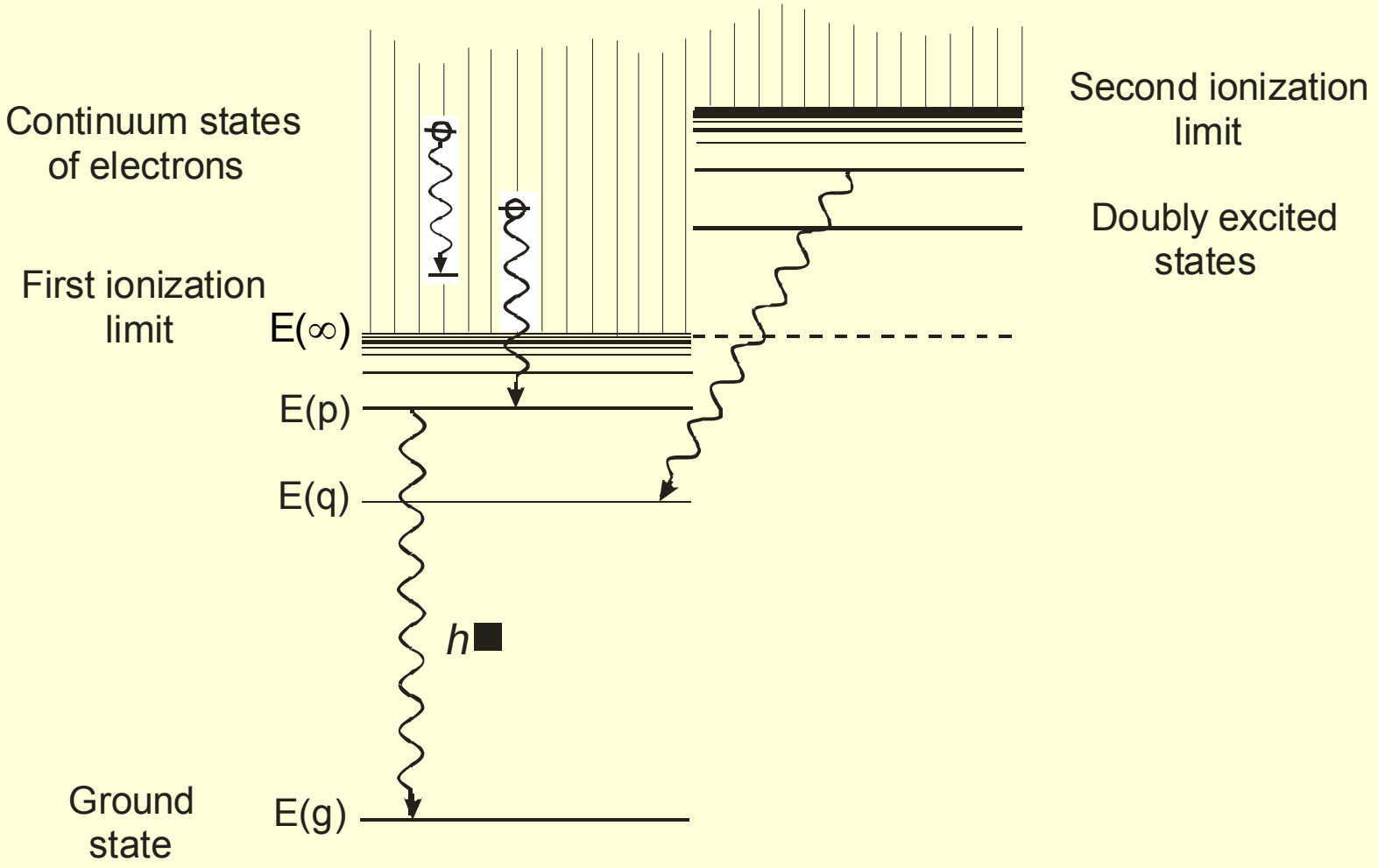

bremsstrahlung free-free transitions

recombination radiation free-bound transitions

line radiation bound-bound transitions

Maximum of bremsstrahlung emission

$$\frac{\lambda_{max}}{\text{nm}} \times \frac{kT_e}{\text{eV}} = 620$$

kT_e = 100 eV $\Rightarrow$ λ_{max} = 6.2 nm $\Rightarrow$ soft x-ray region

Line radiation from ions

present in even in pure hot hydrogen or deuterium plasmas (from walls or deliberately added for *diagnostics* or for *radiation cooling*, sometimes done in fusion devices)

50% of light or medium heavy elements with nuclear charge $6 \le Z_n \le 26$ are completely ionized for

$$\frac{kT_e}{\text{eV}} \ge 0.27\, Z_n^{3.4}$$

Examples: Ar (Z_n = 18) → $kT_e \ge$ 5 keV
C (Z_n = 6) → $kT_e \ge$ 120 eV

Local quantity which characterizes emission

Spectral emission coefficient $\varepsilon_\lambda,\ \varepsilon_\nu,\ \varepsilon_\omega$

defined by

$$\varepsilon_\lambda(\vec{r},\lambda) = \frac{\mathrm{d}^3\Phi}{\mathrm{d}V\ \mathrm{d}\Omega\ \mathrm{d}\lambda}, \quad \text{i.e.} \quad \text{unit} \quad \frac{\mathrm{W}}{\mathrm{m}^3\ \mathrm{sr\ nm}}$$

Φ is the flux out of the volume element dV

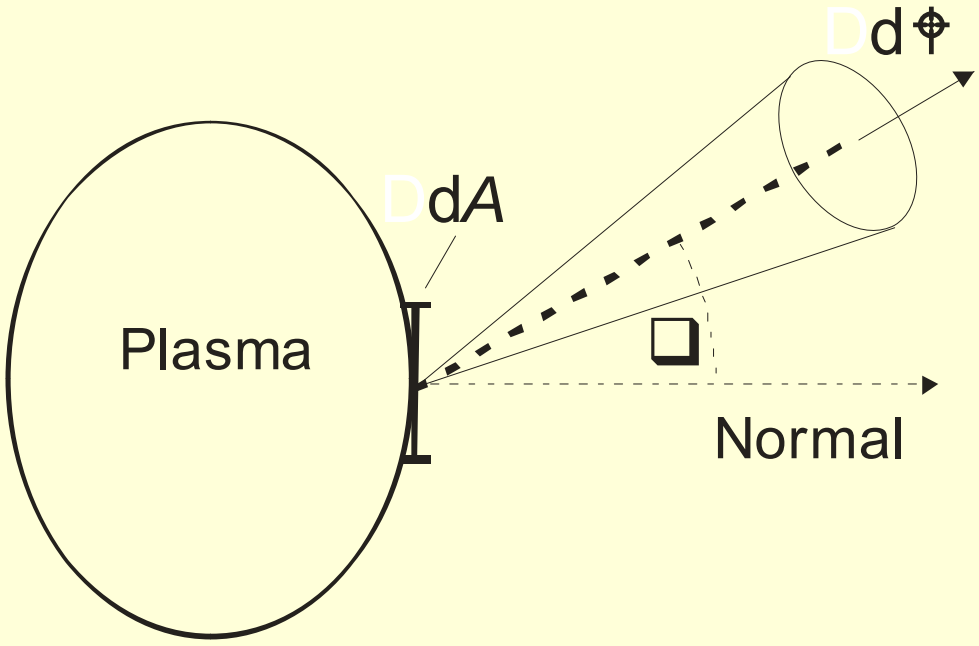

Observation:
Emission from the surface is a flux

Spectral radiance L_λ

(*Intensity !*)

$$L_\lambda = \frac{\mathrm{d}^2\Phi_\lambda}{\mathrm{d}A\cos\theta\,\mathrm{d}\Omega} \qquad \text{unit} \qquad \frac{\mathrm{W}}{\mathrm{m}^2\ \mathrm{sr\ nm}}$$

How does the flux, respectively the radiance, change through the plasma ?

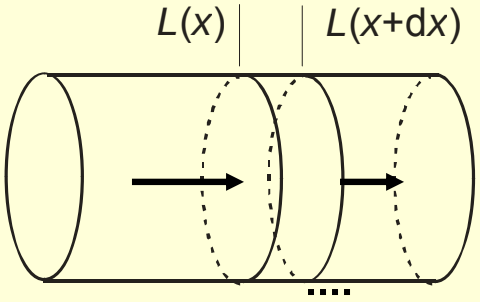

$$\mathrm{d}L_\lambda(x,\lambda) = \varepsilon_\lambda(x,\lambda)\,\mathrm{d}x - \kappa(x,\lambda)L_\lambda(x,\lambda)\,\mathrm{d}x$$

emission absorption

Optical depth $\mathrm{d}\tau = -\kappa(x,\lambda)\,\mathrm{d}x$ $\qquad \tau(x,\lambda) = -\int_0^x \kappa(x',\lambda)\,\mathrm{d}x'$

$$\frac{\mathrm{d}L_\lambda(x,\lambda)}{\mathrm{d}\tau} = L_\lambda(x,\lambda) - \frac{\varepsilon_\lambda(x,\lambda)}{\kappa(x,\lambda)} = L_\lambda(x,\lambda) - S_\lambda(x,\lambda)$$

Equation of radiative transfer $\qquad S_\lambda(x,\lambda)$ source function

Low density plasmas
Hot plasmas

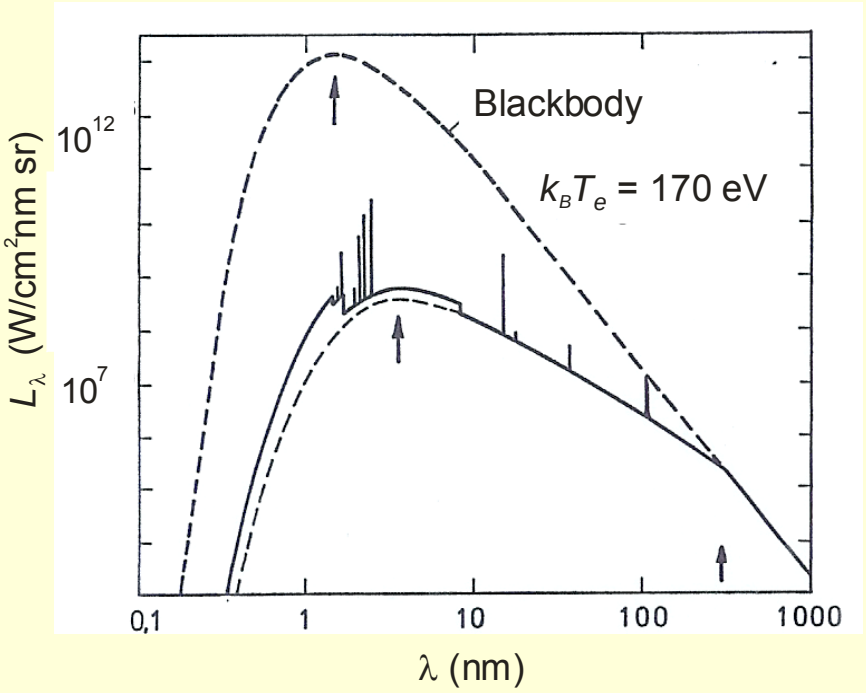

absorption negligible

Spectral radiance at the surface

$$x = 0$$

$$L_\lambda(0,\lambda) = \int_0^{\tau(-\ell,\lambda)} S_\lambda(\tau,\lambda)\,\mathrm{d}\tau$$

$$= \int_{-\ell}^{0} \varepsilon_\lambda(x,\lambda)\,\mathrm{d}x$$

Plasmas become optically thick first at long wavelength !

Lines $\tau(\lambda) \propto n(q) f$

lower state density × oscillator strength

resonance lines !

$$L_\lambda(0,\lambda) = \int_{-\ell}^{0} \varepsilon_\lambda(x,\lambda)\,\mathrm{d}x$$

Drawback of *all* spectroscopic measurements

⟶ information along the line of sight

⟶ Computer tomography

measurements of the radiance in a large number of directions

(practically not possible in plasma devices)

Radial symmetry

Measurement of *L* along many chords

Abel inversion

Local values of $\varepsilon_\lambda(r,\lambda)$

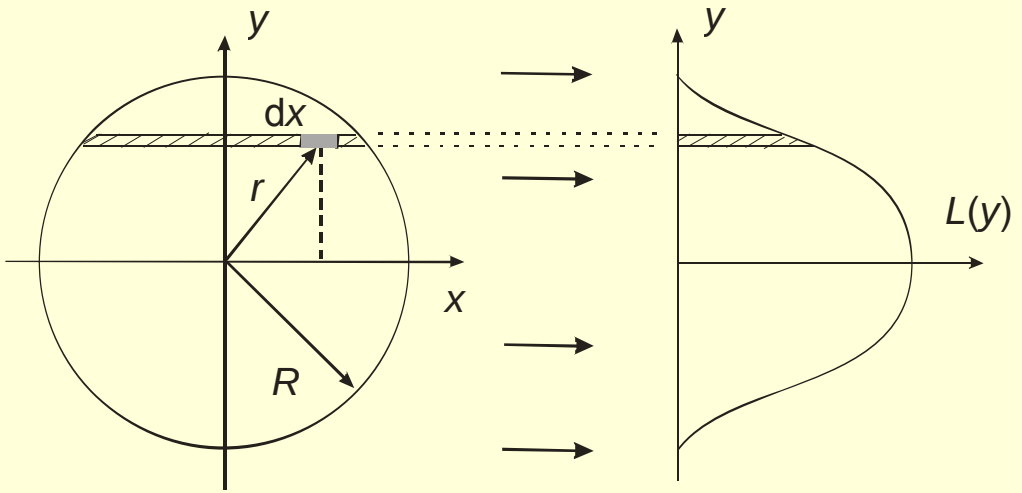

Applicable also to devices with one hole for the measurement

simple transformation

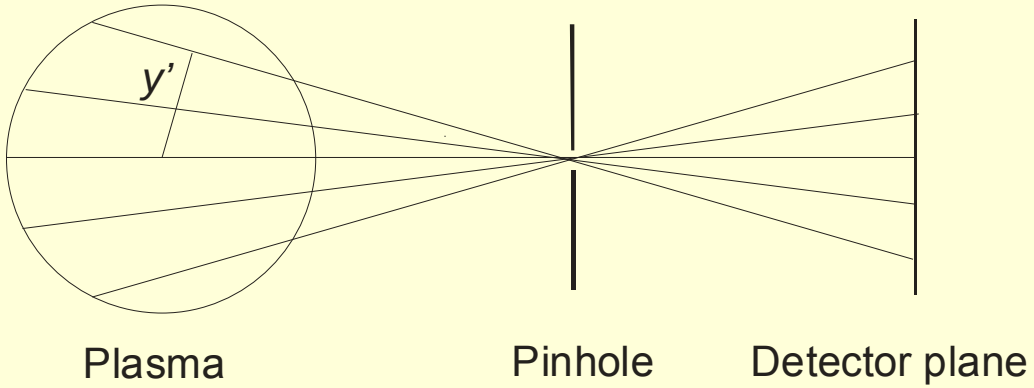

and to tokamaks with a limiter, where density contour lines are very close to a set of nested eccentric circles, the shift being known as Shafranov shift

and to plasmas with elliptic cross-section

(Rev. Sci. Instrum. **63**, 4757 (1992))

Distortion by a thick wall ?

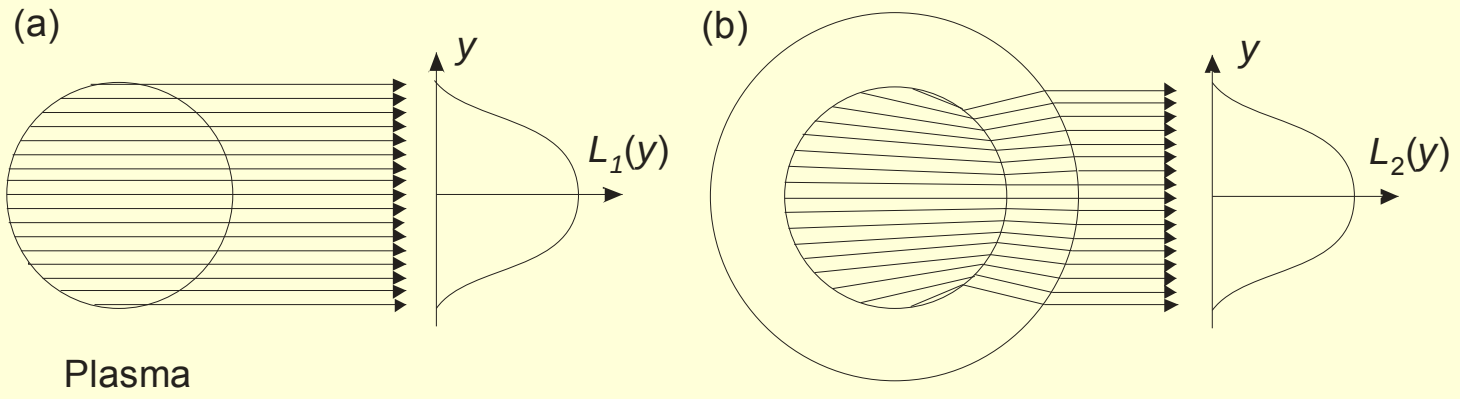

Reflection from the wall ?

(*Wavelength dependent*)

Can cause errors !!

Special case

Beam emission spectroscopy

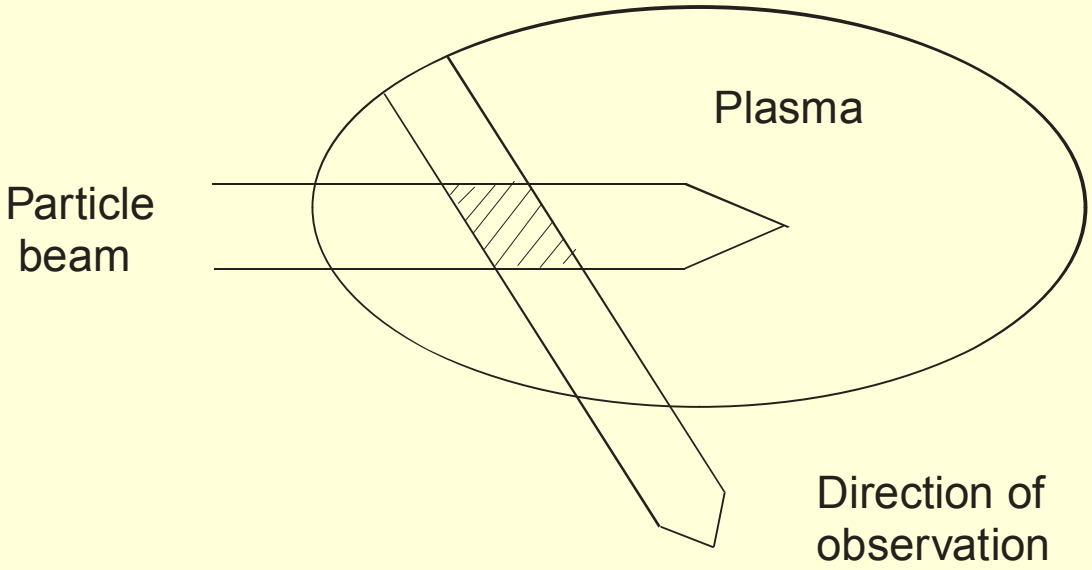

Local information

Li-beams → boundary diagnostics

He- beams

Li-beams (energetic) → magnetic field measurements

H-, D- beams → charge exchange spectroscopy

Let's now assume, we have the local spectral emission coefficient ε_λ in the plasma. What does it tell us?

Continuum radiation

Recombination radiation at long wavelengths becomes negligible

Bremsstrahlung at long wavelengths for a pure hydrogen plasma

$$\varepsilon_\lambda^{ff}(\lambda) \sim \frac{1}{\lambda^2} \frac{n_e^2}{(k_B T_e)^{1/2}}$$

Weak temperature dependence, strong electron density dependence → electron density diagnostics

With impurities:

$$\varepsilon_\lambda^{ff}(\lambda) \sim \frac{1}{\lambda^2} \frac{n_e \sum_{i,z} z_i^2 n_z^i}{(k_B T_e)^{1/2}}$$

All impurity ions of charge z contribute

Deviation of the emission coefficient from that of a pure H-plasma is a measure of the impurity contamination characterized in fusion plasmas by

$$\varepsilon_\lambda^{ff}(\lambda) = Z_{eff}\ \varepsilon_\lambda^{ff}(\lambda)(H)$$

Z_{eff} is some kind of a mean charge

At high densities plasmas become optically thick at long wavelengths ⟶ emission corresponds to that of a blackbody ⟶ temperature

At short wavelengths

both bremsstrahlung and recombination radiation

exponential dependence in frequency

$$\lg \varepsilon_\nu(\nu) \simeq \frac{1}{\ln 10}\frac{h\nu}{k_B T_e} + const$$

Slope of straight line gives T_e

Bremsstrahlung and Recombination radiation

$$e^{-\frac{h\nu}{k_B T_e}}$$

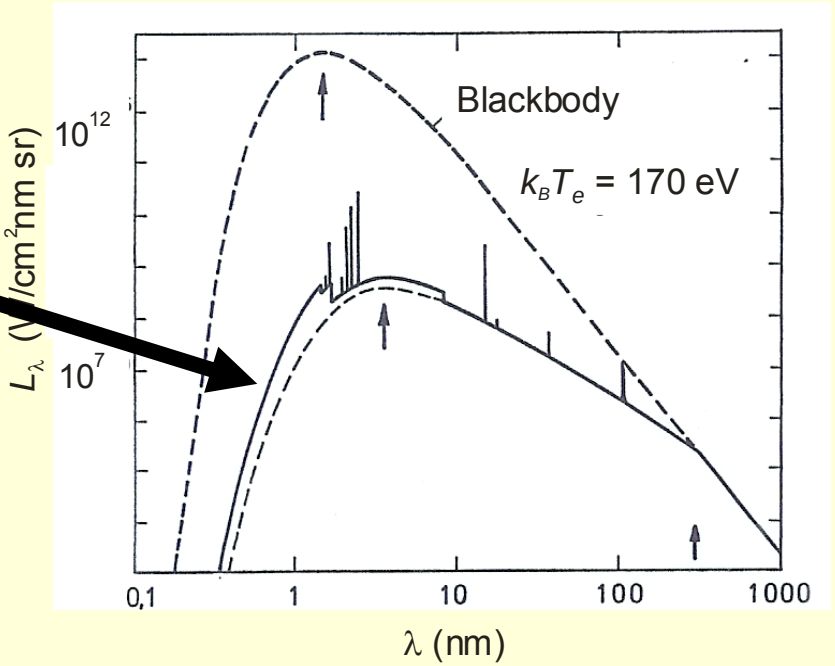

Examples

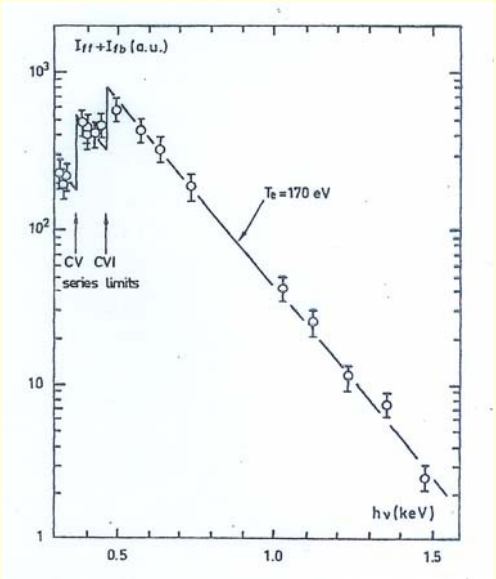

Laser-produced plasma

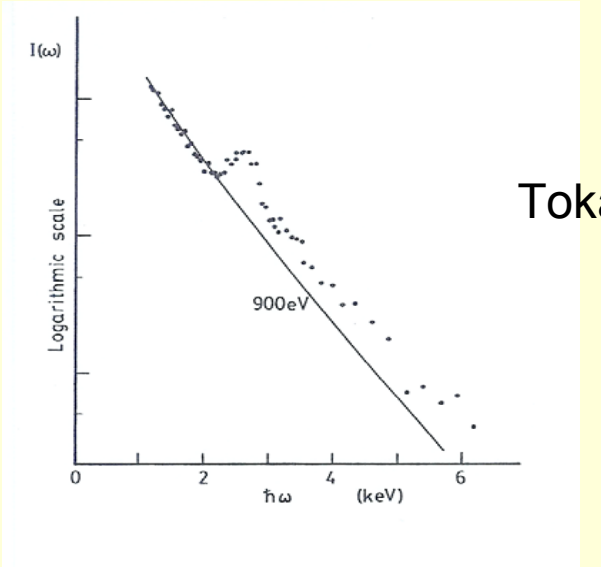

Tokamak

M. Galanti and N. J. Peacock
J. Phys. B **8**, 2427 (1975)

J. E. Rice, K. Molvig, H. I. Helava,
Phys. Rev. A **25**, 1645 (1982)

Line radiation

Emission coefficient of a line between upper level p and lower level q

$$\varepsilon(\nu) = \frac{h\nu}{4\pi} A(p \to q)\, n_z(p)$$

$A(p \to q)$ is the transition probability

The quantity obtained thus is the population density $n_z(p)$ of the upper level

Theoretical considerations are needed to establish how $n_z(p)$ is determined by the parameters of the plasma

General approach:

One has to look at the rate equation:

$$\frac{\mathrm{d}n_z(p)}{\mathrm{d}t} = - n_z(p) \sum_{q \neq p} n_e X_z(p \to q) + \sum_{q \neq p} n_z(q)\, n_e X_z(q \to p)$$
$$- n_z(p) \sum_{q<p} A_z(p \to q) + \sum_{r>p} n_z(r)\, A_z(r \to p)$$
$$- n_z(p)\, n_e S_z(p \to g) + n_{z+1}(g)\, n_e^2\, \alpha^{cr}_{z+1}(g \to p)$$
$$+ n_{z+1}(g)\, n_e\, \alpha^{rr}_{z+1}(g \to p)$$
$$+ n_{z+1}(g)\, n_e\, \alpha^{dr}_{z+1}(g \to p)\,.$$

$A(p \to q)$: *radiative transitions*

$n_e X_z(g \to p)$: *electron collisional transitions*

$n_e S_z(p \to g)$: *electron collisional ionization*

$n_e^2 \alpha^{cr}_{z+1}(g \to p)$: *collisional recombination*

$n_e \alpha^{rr}_{z+1}(g \to p)$: *radiative recombination*

$n_e \alpha^{dr}_{z+1}(g \to p)$: *dielectronic recombination*

Proton collisions, photo-excitation and photo-ionization are neglected

X, S, and α are rate coefficients, *i.e.*

$$\langle \sigma v \rangle = \int \sigma \, v \, f_e(v) \mathrm{d}v$$

This means, that in some cases high energy tails of the distribution function may markedly influence population densities and may thus be detected

Looking at time scales allows simplification in most cases:

Time scales of ionization and recombination are long compared to relaxation of excited level populations, which are at least given by 1/A.

One solves separately the rate equation of ionization/recombination

$$\frac{\mathrm{d}n_z(g)}{\mathrm{d}t} = -n_e n_z(g) S_z^{eff}(T_e, n_e) + n_e n_{z+1}(g) \alpha_{z+1}^{eff}(T_e, n_e)$$

and $$\frac{dn_z(p)}{dt} = 0 \quad for \quad p > g$$

means

Excited levels are in quasi-equilibrium with their ground states, they follow instantaneously their ground state density

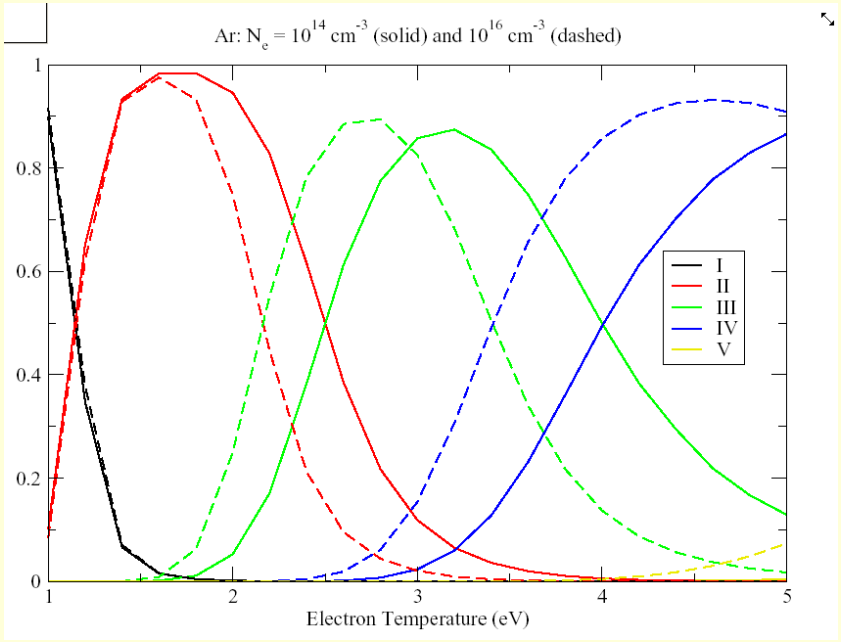

Distribution of ionization stages calculated for 2 densities: Increasing density shifts Ionization to lower stages

In *transient plasmas*: atoms go successively through their ionization stages till they reach equilibrium

Maximum abundance of an ion gives rough estimate of temperature at low densities

Simplification at low and high densities !

Dielectronic recombination

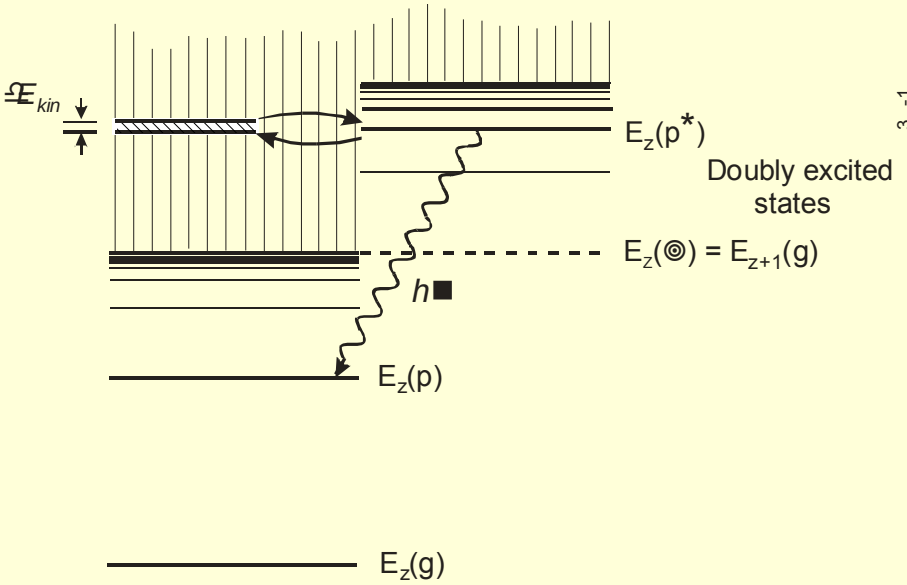

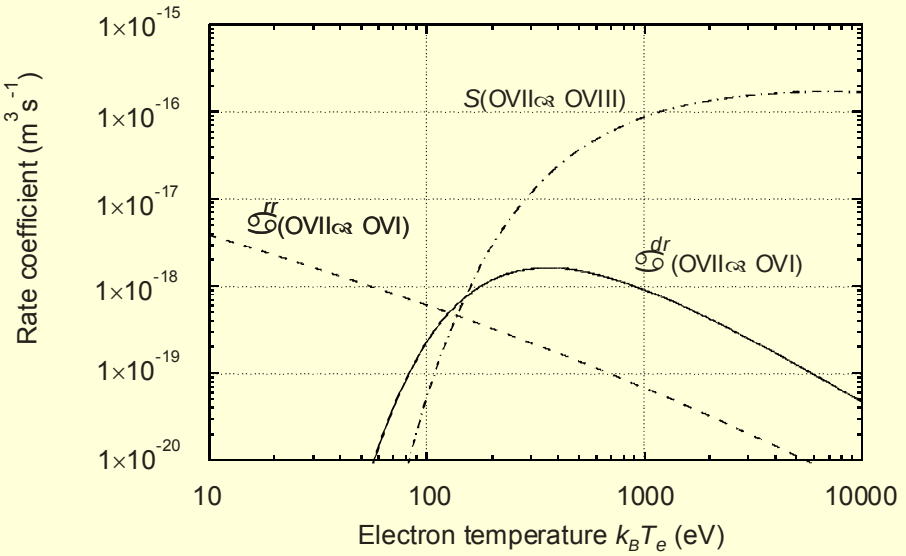

Dielectronic capture followed by a stabilizing transition (satellites !)

High densities: electron collisions dominate and establish a population equilibrium between the levels, which corresponds to that of thermodynamic equilibrium.
It is called local thermodynamic equilibrium (LTE)
(no equilibrium with the radiation field).

Advantage: Equilibrium relations can be applied.

Boltzmann distribution:

$$\frac{n_z(p)}{n_z(q)} = \frac{g_z(p)}{g_z(q)} \exp\left[- \frac{E_z(p) - E_z(q)}{k_B T_e} \right]$$

Saha-Eggert equation:

$$\frac{n_{z+1}(g)\, n_e}{n_z(q)} = \frac{g_{z+1}(g)}{g_z(q)} \frac{1}{\lambda_B^3} \exp\left(- \frac{E_{z,q\infty}}{k_B T} \right) \quad \text{mit} \quad \lambda_B = \left(\frac{2\pi\hbar}{m_e k_B T} \right)^{1/2}$$

$$\frac{n_{z+1} n_e}{n_z} = 2 \frac{U_{z+1}(T)}{U_z(T)} \frac{1}{\lambda_B^3} \exp\left(- \frac{E_{z,g\infty}}{k_B T} \right)$$

$g_z(p)$ statistical weight of level (p) of ion (z)
$U_z(T)$ partition function of ion (z)
λ_B thermal deBroglie wavelength

With decreasing electron density collisional coupling ceases to exist first between levels with the largest energy separation, which in many cases is between ground state and excited state

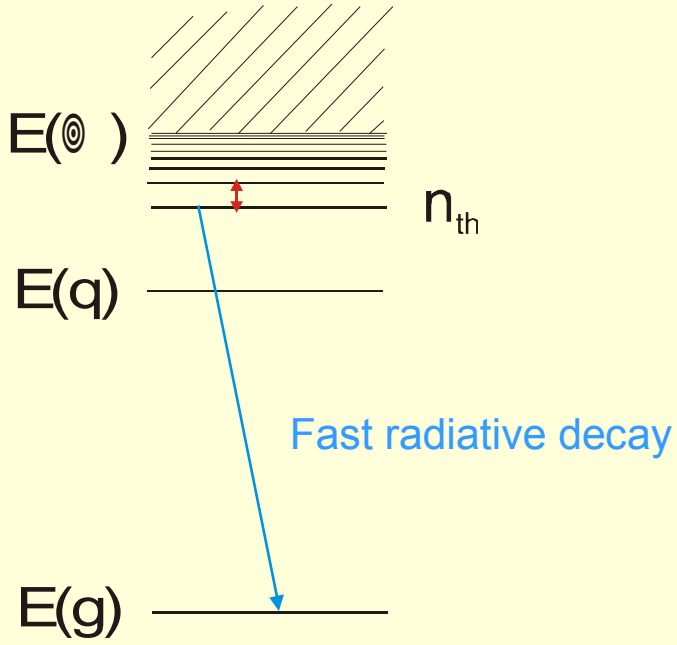

n_{th} thermal level

above n_{th} equilibrium relations still prevail

Partial local thermodynamic equilibrium (PLTE)

Low densities

Collisional processes are weak, radiative ones dominate

Excitation of levels is typically from the ground state (maybe from a metastable state) by electron collisions, depopulation by radiative decay

$$n_z(g)\, n_e X(g \rightarrow p; T_e) = n_z(p)\, A(p \rightarrow)$$

$$n_z(p) = n_z(g)\, \frac{n_e X(g \rightarrow p; T_e)}{A(p \rightarrow)} = f(n_e, T_e)$$

Excited state populations are low, most ions are in the ground state or in a metastable state

Low density limit is also called corona approximation

Distribution of the ions:

$$n_z n_e S_z(T_e) = n_{z+1} n_e (\alpha^{rr}_{z+1} + \alpha^{dr}_{z+1})$$

$$\frac{n_{z+1}}{n_z} = \frac{S_z(T_e)}{\alpha^{rr}_{z+1}(T_e) + \alpha^{dr}_{z+1}(T_e)} = f(T_e)$$

known as corona distribution

Examples of spectroscopic methods

employing the fundamental equation $\varepsilon(p \to q) = \frac{h\nu_{pq}}{4\pi} A(p \to q)\, n_z(p)$

$$n_z(p) = \frac{4\pi\ \varepsilon(p \to q)}{h\nu_{pq} A_z(p \to q)}$$

Particle densities n_z

At high densities with LTE satisfied for the ion:

$$n_z = \frac{n_z(p)}{g_z(p)} U_z(T_e) \exp\left[+\frac{E_z(p) - E_z(q)}{k_B T_e}\right]$$

$$= \frac{4\pi\ \varepsilon(p \to q)}{h\nu_{pq} A_z(p \to q)} \frac{U_z(T_e)}{g_z(p)} \exp\left[\frac{h\nu_{pq}}{k_B T_e}\right]$$

T_e and partition function $U_z(T_e)$ must be known to obtain n_z!

In case the upper level is in PLTE, the Saha Eggert equation yields

$$n_{z+1}(g) = \frac{4\pi\,\varepsilon_z(p \to q)}{h\nu_{pq} A_z(p \to q)} \frac{2g_{z+1}(g)}{g_z(p)} \frac{1}{n_e} \left(\frac{m_e k_B T_e}{2\pi\hbar^2} \right)^{3/2} \exp\left(-\frac{E_{z,p\infty}}{k_B T_e} \right)$$

Now also the electron density n_e must be known, in addition.

At low densities in the coronal regime

$$n_z \simeq n_z(g) = \frac{A_z(p \to)}{n_e X_z(g \to p)} n_z(p)$$

$$= \frac{4\pi\,\varepsilon_z(p \to q)}{h\nu_{pq} A_z(p \to q)} \frac{A_z(p \to q)}{n_e X_z(g \to p; T_e)}$$

Forbidden transitions of the M1-type between fine structure levels of the ground state of highly ionized atoms.

Electron and proton collisions are fast enough to establish equilibrium population distribution given simply by the statistical weigths

Thus one line suffices to calculate n_z,

neither n_e nor T_e must be known

Further advantage: lines of many ions are in the visible.

Examples are the green and red iron lines of FeXIV and FeXV observed first in the solar corona, now used in many tokamaks

Charge exchange with injected fast beams of hydrogen is an indispensable tool to measure the ♋-particles produced in a burning plasma (local).

$$n_z(p)\,A(p\rightarrow) = \langle \sigma^{cx}(v)\,v \rangle\, n_{z+1} n_b$$

Charge exchange is selectively into levels of high principal quantum number and there into high *l*, decay via 👎n_p=-1 transitions at long wavelengths

Helium-like ions

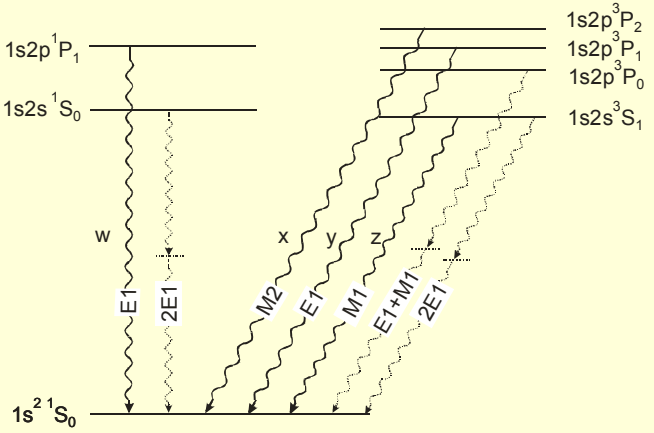

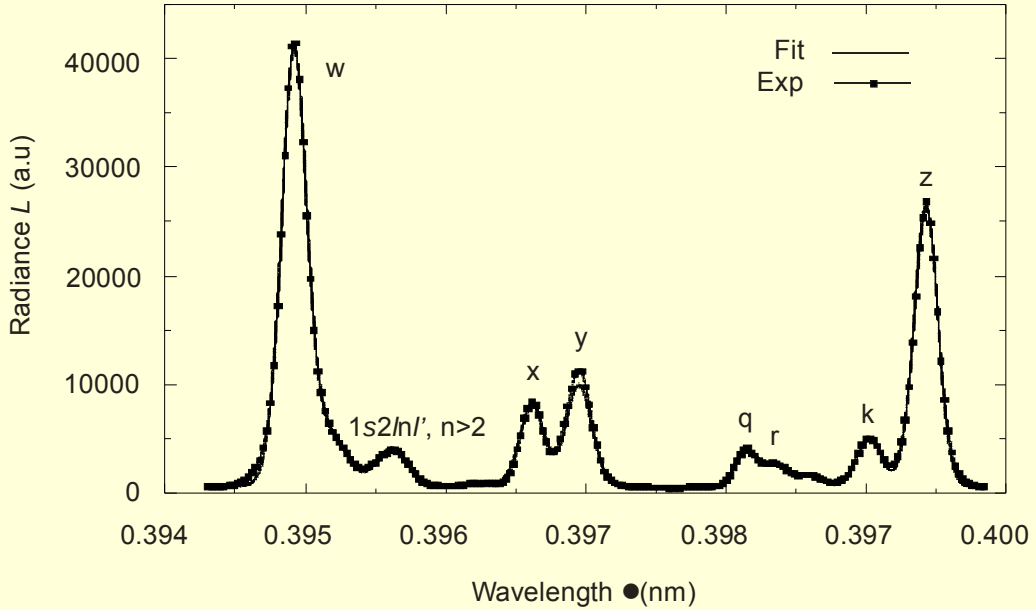

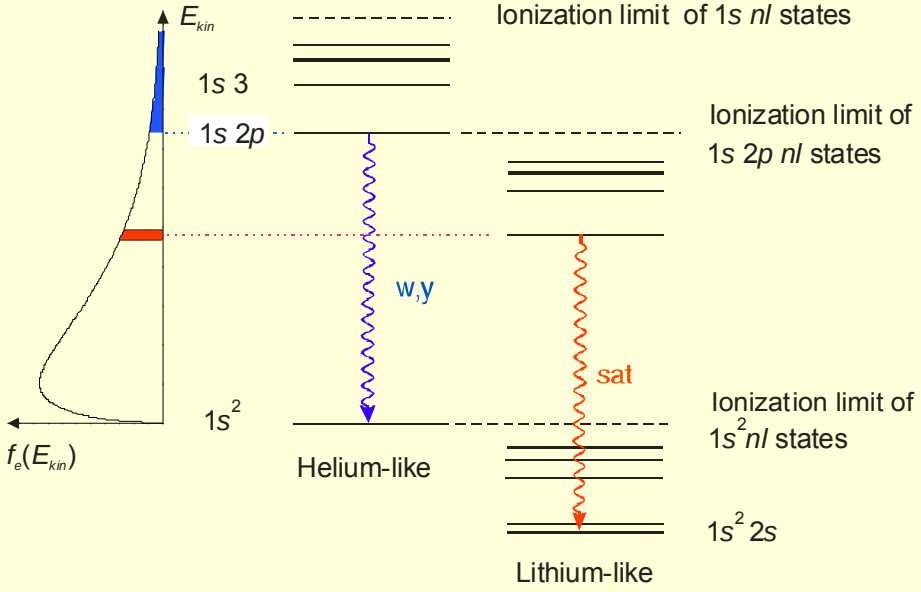

w: resonance line
y: intercombination line
x,z: forbidden lines

Dielectronic and innershell excited satellites

all close in wavelength

Resonance line: $\varepsilon_w \propto n_e \, X_w(T_e)\, n_{He}(g)$

Dielectronic satellite $\varepsilon_{sat}^{dr} \propto n_e \, \alpha_{He}^{dr}(T_e)\, n_{He}(g)$

Innershell excitation $\varepsilon_{sat}^{in} \propto n_e \, X^{in}(T_e)\, n_{Li}$

$$\frac{\varepsilon_{sat}^{dr}}{\varepsilon_w} = F_1(T_e)$$

$$\frac{\varepsilon_{sat}^{in}}{\varepsilon_w} \propto F_2(T_e)\,\frac{n_{Li}}{n_{He}}$$

The z-line is essentially populated by recombination of the hydrogenlike ion:

$$\frac{\varepsilon_z}{\varepsilon_w} \propto F_3(T_e)\,\frac{n_H}{n_{He}}$$

Such spectra of heavy helium-like ions are now much used in *tokamak plasmas (*up to Ni*)*. They are in the x-ray region. Look at the nice fit !!

Electron temperature

One example for low densities we just have seen.

Taking line ratios is convenient since the ground state density and the electron density drop

$$\frac{\varepsilon_z(p \to q)}{\varepsilon_z(p' \to q')} = \frac{\lambda_{p'q'}}{\lambda_{pq}} \frac{A_z(p \to q)}{A_z(p' \to q')} \frac{A_z(p' \to)}{A_z(p \to)} \frac{X_z(g \to p)}{X_z(g \to p')} = f(T_e)$$

You need to know the excitation functions !

With increasing density, ratios become also dependent on the electron density and one has to use, in general, collisional-radiative models

Ratios become simple at high densities, when the upper level populations are described by a Boltzmann distribution
Check for condition !

$$\frac{\varepsilon_z(p \to q)}{\varepsilon_z(p' \to q')} = \frac{\lambda_{p'q'}}{\lambda_{pq}} \frac{A_z(p \to q)}{A_z(p' \to q')} \frac{g_z(p)}{g_z(p')} \exp\left[- \frac{E_z(p) - E_z(p')}{k_B T_e} \right]$$

Instead of several line pairs:

calculate the population densities $n_z(p)$ of the upper levels, and plot $\lg[n_z(p)]$ versus the energy $E_z(p)$

⟶ Boltzmann plot

Straight line, the slope gives T_e

For high sensitivity energy separation of levels should be large !

Lines from successive ionization stages

For example: Saha-Eggert equation connects population of upper level (p') of ion (z) with population of ground state of ion (z+1), and Boltzmann relation connects that with the Population density $n_{z+1}(p)$ of level (p) in that ion

A number of examples are found in the literature.
Drawback: valid only in some high density range

Electron density

From line ratios

Select one line with an upper level (p) decaying essentially only by radiation to the ground state,
and another line where the upper level (p') is also depopulated by collisions

$$n_z(g)\, n_e\, X_z(g \to p) \simeq n_z(p)\, A(p \to)$$

$$n_z(g)\, n_e\, X_z(g \to p') \simeq n_z(p')\left[A(p' \to) + X_z(p' \to)\right]$$

$$\frac{\varepsilon_z(p \to q)}{\varepsilon_z(p' \to q')} \cong \frac{\lambda_{p'q'}}{\lambda_{pq}} \frac{A_z(p \to q)}{A_z(p \to)} \frac{A_z(p' \to)}{A_z(p' \to q')} \frac{X_z(g \to p)}{X_z(g \to p')}$$

$$\times \left[1 + n_e \frac{X_z(p' \to)}{A_z(p' \to)}\right]$$

Example

Ratio of intercombination and resonance line in helium-like ions
(often used in laser-produced plasmas)

Spectral lines are broadened
natural broadening
Doppler broadening
Stark broadening
van der Waals broadening
resonance broadening

$$\varepsilon_\lambda(\lambda) = \varepsilon(p \to q)\, \ddot{E}(\lambda)$$

$$\int_{-\infty}^{\infty} \ddot{E}(\lambda)\, \mathrm{d}\lambda = 1$$

$\ddot{E}(\lambda)$ line profile, line shape function

Natural broadening is typically negligibly small

Stark broadening (pressure broadening) is by charged plasma particles (electrons and ions). Their electric field leads to broadening of the levels.

Two approximations are usually employed to calculate the broadening. Very difficult to calculate in general, so this was to benefit of the experimentalists who had to furnish experimental verifications

Impact approximation and *quasistatic approximation*

Impact approximation: electric field produced by the electrons varies so rapidly at the position of the radiator, that the effect can be treated as collision.

In cases, where the broadening effect on the lower state can be neglected (one-state version), the half-width of a line is

$$\Delta\omega_{1/2} \simeq n_e X(p),$$

where X(p) stands for the sum of elastic and inelastic collisions.

Collisions with neighboring fine structure levels usually being strongest leads to

$$\Delta\omega_{1/2} \propto \frac{n_e}{(T_e)^x} \qquad \textit{with} \qquad 0.2 < x < 0.5$$

(weak temperature dependence)

Lines are also shifted! In principle, it also can be used for density diagnostics, but it is less accurate!

Broadening data (including the corrections by the ion contributions) are found in the book by Griem (Spectral Broadening by Plasmas, Academic Press, 1974)

A comprehensive bibliographic data bank is maintained at NIST

http://physics.nist.gov/cgi-bin/ASBib1/LineBroadBib.cgi

Profiles have a Lorentzian shape

Quasistatic approximation:

The field produced by the ions is considered static during the emission process. This microfield splits and shifts upper and lower levels by the Stark effect. Perturbation theory gives

$$\Delta\omega_{pq}(E) = C_{pq}^{k}\, E^{m},$$

where m=1 and m=2 holds for linear and quadratic Stark effect and (k) designates the Stark component. First calculation of the microfield was by Holtsmark, new calculations are mostly for high densities. The line profiles mirror the microfield distribution, certainly slightly modified by electron collision contributions

Because the linear Stark effect is much stronger than the quadratic Stark effect, the quasistatic approximation is appropriate for hydrogen and hydrogenic ions.

Theory is still being improved, and good measurements are needed for comparison

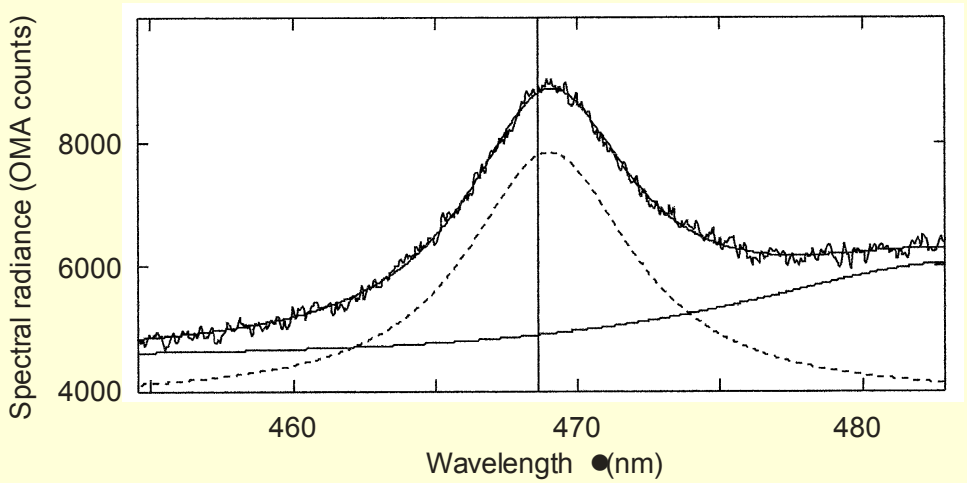

Paschen-♋ line of HeII at 468.6 nm measured for n_e= 3.5 x 10^{24} m^{-3}
$k_B T_e$= 6.8 eV

$$\frac{\Delta\lambda_{1/2}}{\text{nm}} \simeq 2.74\times10^{-20}\left(\frac{n_e}{\text{m}^{-3}}\right)^{0.831}$$

With increasing principal quantum number n_p of upper levels lines become broader and finally merge → Inglis Teller limit

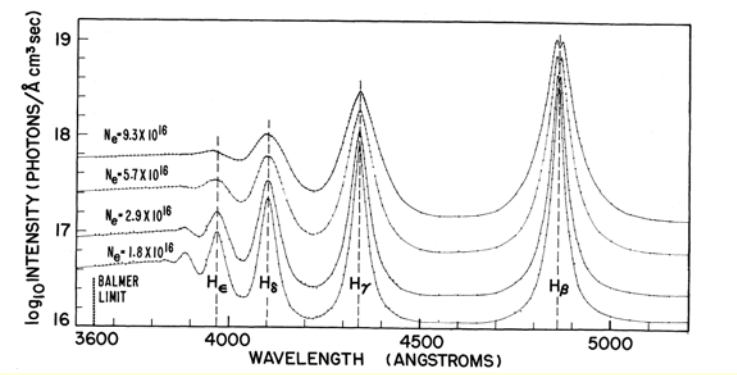

H Balmer series

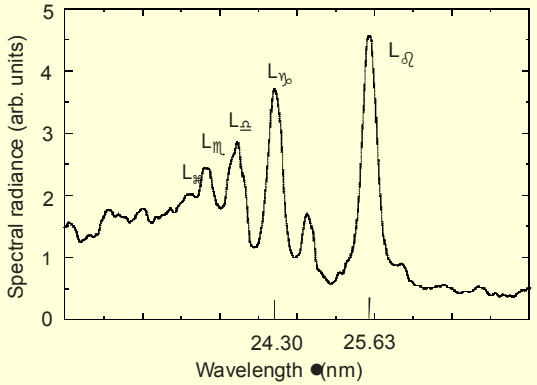

He Lyman series

Allows estimate of the perturber density

$$\lg \frac{n_z}{\mathrm{m}^{-3}} \approx 29.12 + 4.5 \lg Z - 1.5 \lg z - 7.5 \lg n_{p,\max}$$

Lines with forbidden components (e.g. HeI lines)

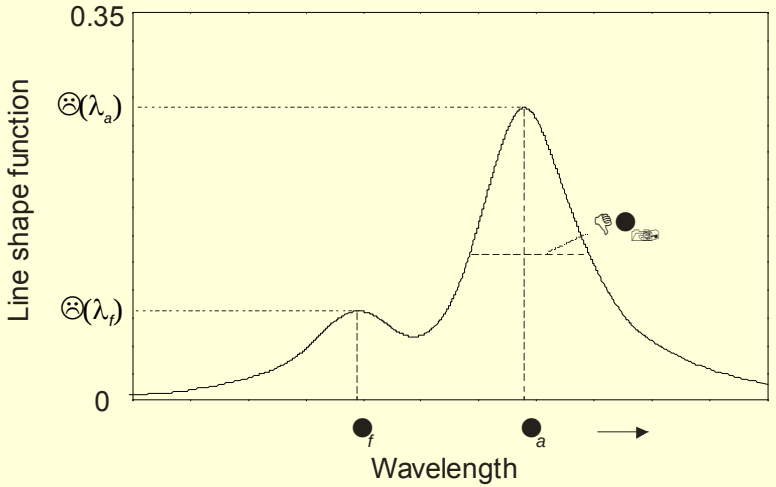

Electric field increasing with density mixes wave-functions of upper levels

→ forbidden lines increase

Particle temperature T_z

Motion of an emitter results in Doppler shift of emitted lines

$$\frac{\omega - \omega_{pq}}{\omega_{pq}} = \frac{v_x}{c},$$

where v_x is the velocity component in the direction x of emission, and c is the speed of light.

Line profile and velocity distribution function are related by

$$\ddot{E}_D(\omega)\,\mathrm{d}\omega = f_z(v_x)\,\mathrm{d}v_x$$

The line profile thus mirrors $f_z(v_x)$, and if this is Maxwellian, the profile has a Gaussian shape ⟶
half width gives T_z

$$\frac{\Delta\lambda_{1/2}}{\lambda_{pq}} = 7.715\times10^{-5}\sqrt{\frac{k_B T_z / \mathrm{eV}}{m_z / \mathrm{u}}}$$

Magnetic field measurements

Magnetic fields split lines into their Zeeman components which gives, in principle, the magnetic field, if Doppler broadening does not dominate

$$\frac{\Delta\lambda^{split}}{\Delta\lambda_{1/2}} \propto \lambda_{pq} \frac{B}{\left(k_B T_z / m_z\right)^{1/2}}$$

This suggests to use long wavelength transitions (large λ_{pq}) in heavy ions (large m_z)

→ magnetic dipole transitions between fine structure level of the ground state

→ $2^2P \rightarrow 2^2S$ transition of injected high-energy Li-beams at 670.8 nm

Motional Stark effect

Fast beams (e.g. injected hydrogen heating beams) experience the Lorentz electric field

$$\vec{E} = \vec{v_b} \times \vec{B}$$

in their rest frame.

This gives a Stark-Zeeman pattern, where the Zeeman splitting can be smaller than the Stark splitting.

For diagnostics usually the Balmer-♋ line of hydrogen (deuterium) is employed. Excitation is primarily by *proton collisions* from the ground state.

Use is made also of the polarization characteristics

Early example

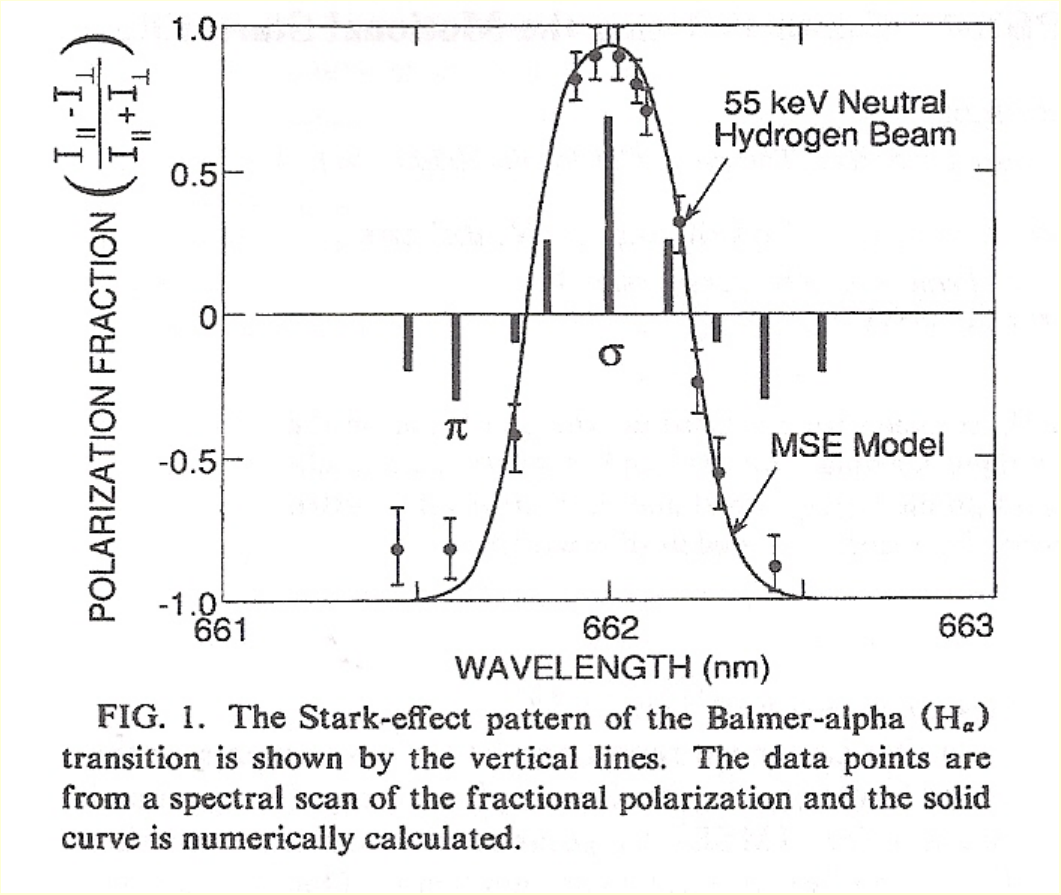

FIG. 1. The Stark-effect pattern of the Balmer-alpha (H_α) transition is shown by the vertical lines. The data points are from a spectral scan of the fractional polarization and the solid curve is numerically calculated.

Levinton et al. Phys. Rev. Lett. 63, 2060 (1989)

Some experimental mistakes found in publications

- No accurate wavelength calibration
- No spectral sensitivity calibration (authors simply used reflectivity data of grating, mirror, detector)
- No absolute sensitivity calibration
- Neglect of sensitivity change across a two-dimensional detector (vignetting in the optical path, pixel to pixel variation)
- No check on the optical thickness of lines (authors even published change of transition probabilities at high densities because of this neglect)
- Neglect of damping on signals in cables
- Fast gating (irising effect): due to finite travel time of gating pulse delay in switching from center to edge)
- Saturation of detectors
- Use of a system outside its sensitivy/design range

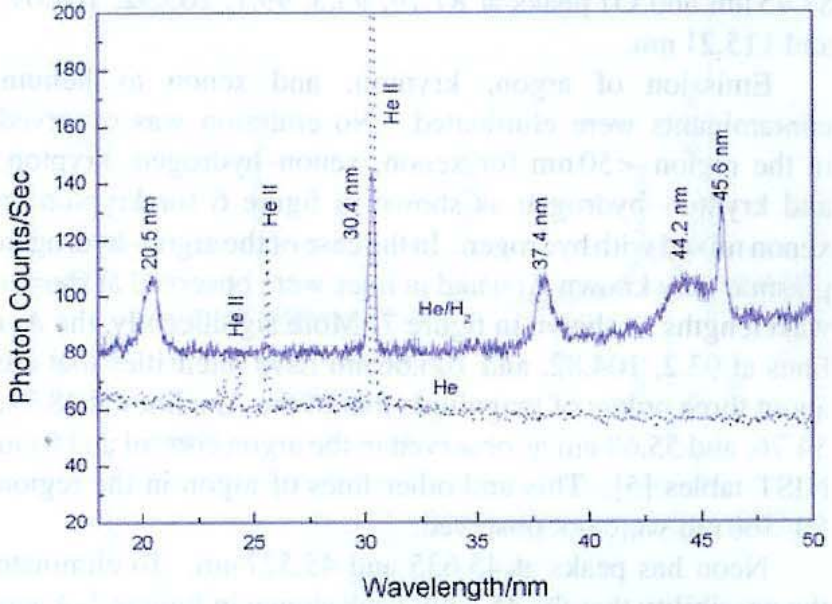

Figure 2. The EUV spectra (17.5–50 nm) of the microwave cell emission of the helium–hydrogen mixture (98/2%) (top curve) recorded at 20 Torr with a normal incidence EUV spectrometer and a CEM, and control helium (bottom curve) recorded at 20 Torr with a 4° grazing incidence EUV spectrometer and a CEM. Only known He I and He II peaks were observed with the helium control. Reproducible novel emission lines were observed at 45.6 and 30.4 nm with energies of $q \cdot 13.6$ eV, $q = 2$ or 3 (equations (2*a*) and (2*c*)) and at 37.4 and 20.5 nm with initial energies of $q \cdot 13.6$ eV. $q = 4$ or 6 that were inelastically scattered by helium atoms wherein 21.2 eV was absorbed in the excitation of He ($1s^2$) to He ($1s^1 2p^1$) as proposed in equation (8).

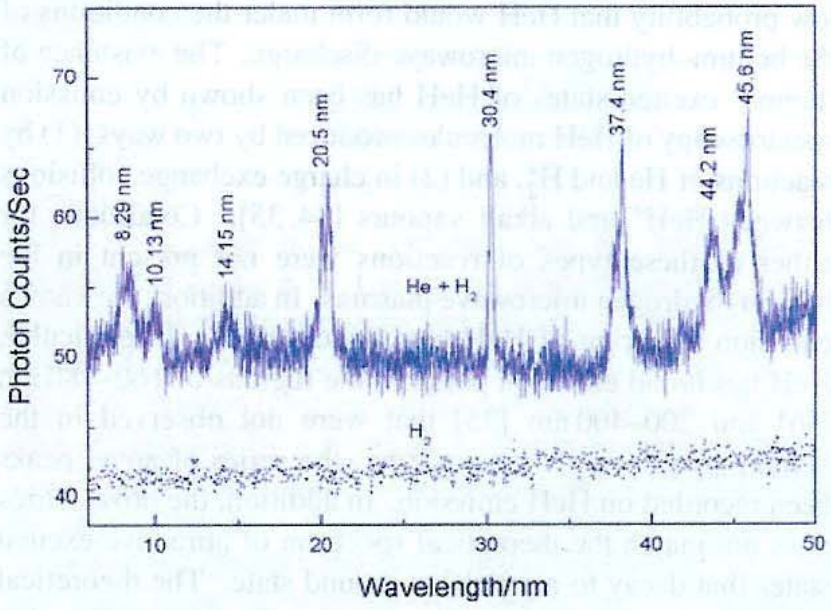

Figure 4. The short wavelength EUV spectra (5–50 nm) of the microwave cell emission of the helium–hydrogen mixture (98/2%) (top curve) and control hydrogen (bottom curve) recorded at 1 Torr with a normal incidence EUV spectrometer and a CEM. No hydrogen emission was observed in this region, and no instrument artefacts were observed. Reproducible novel emission lines were observed at 45.6, 30.4, 13.03, 10.13, and 8.29 nm with energies of $q \cdot 13.6$ eV, $q = 2, 3, 7, 9$, or 11 and at 37.4, 20.5 nm, and 14.15 nm with initial energies of $q \cdot 13.6$ eV, $q = 4, 6$, or 8 that were inelastically scattered by helium atoms wherein 21.2 eV was absorbed in the excitation of He ($1s^2$) to He ($1s^1 2p^1$) as proposed in equation (8). The peak at 13.03 nm was observed as a weak shoulder on the 14.15 nm peak, and has been observed in repeated (nonpresented) spectra.

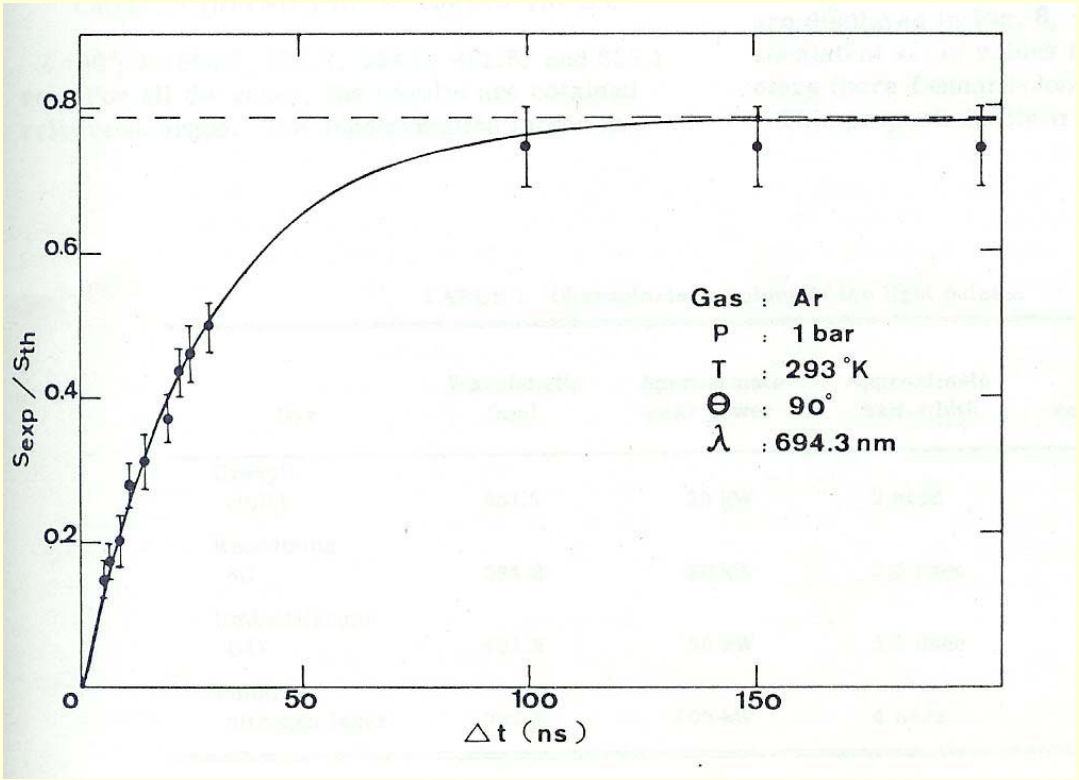

Phys. Rev. A **19**, 2260 (1978)

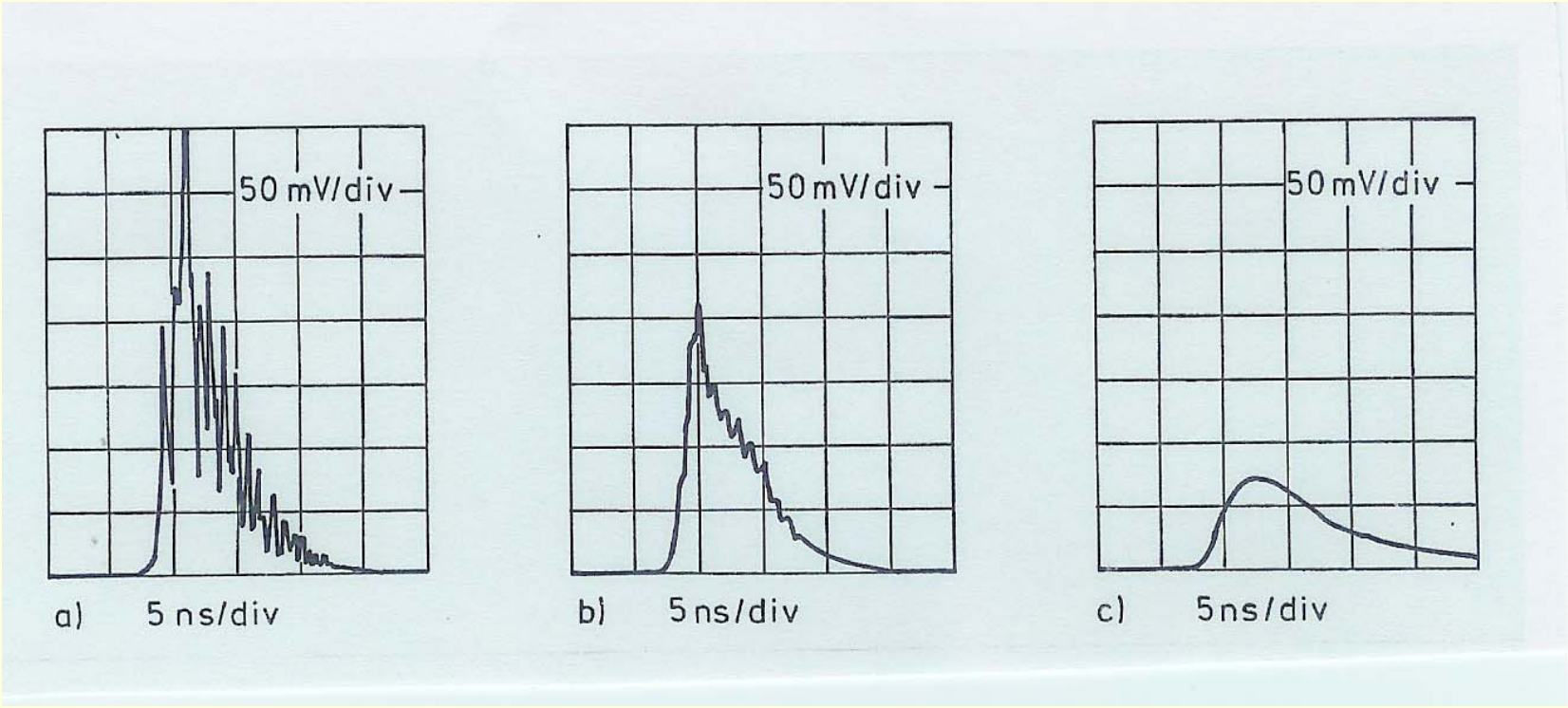

Signal from a photodiode recorded with a fast oscilloscope with a cable RG 58 C/U
a) 1 m long b) 11 m long c) 79 m long

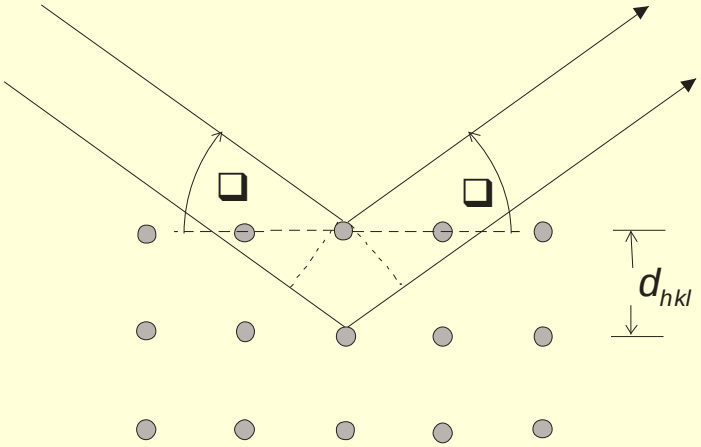

Bragg condition

$$m\lambda = 2d_{hkl}\sin\theta$$

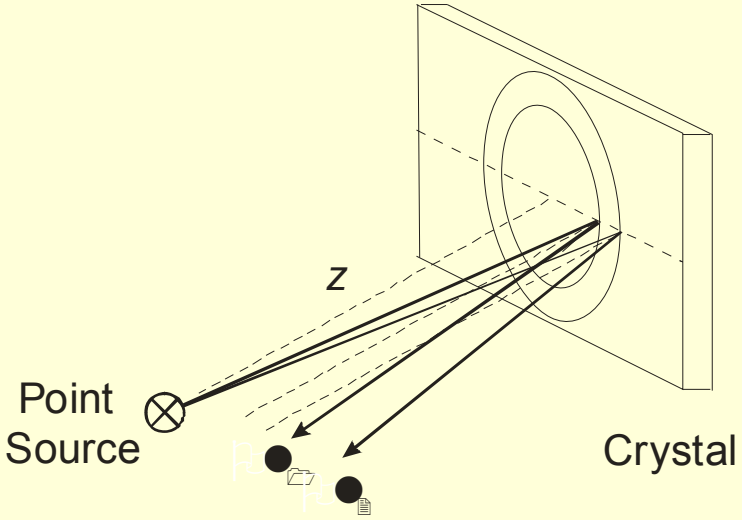

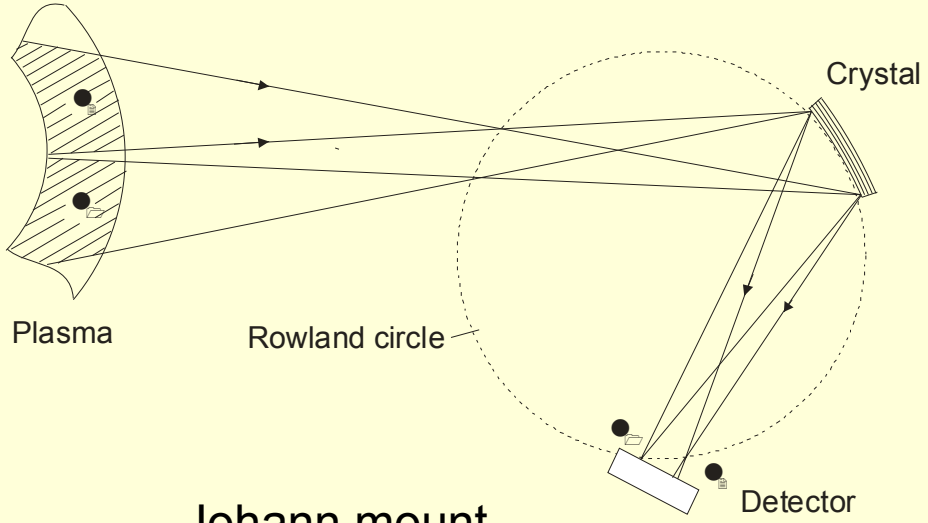

Johann mount

cylindrically, spherically bent

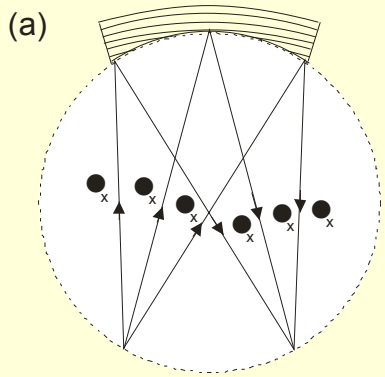

Johansson

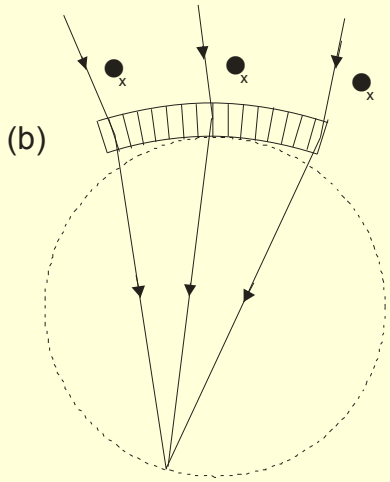

Cauchois mount

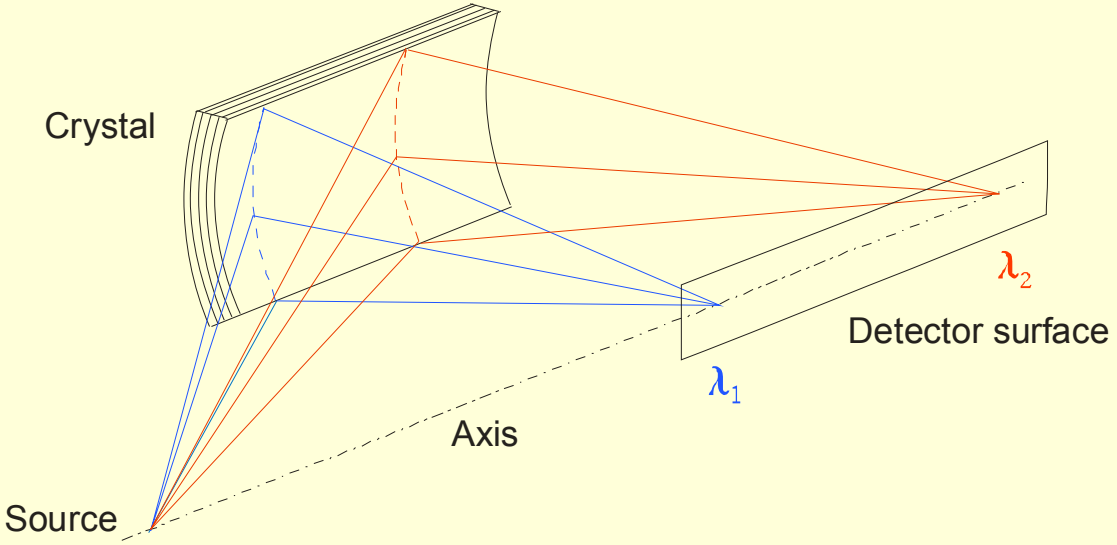

Van Hamos mount

EUV spectral region

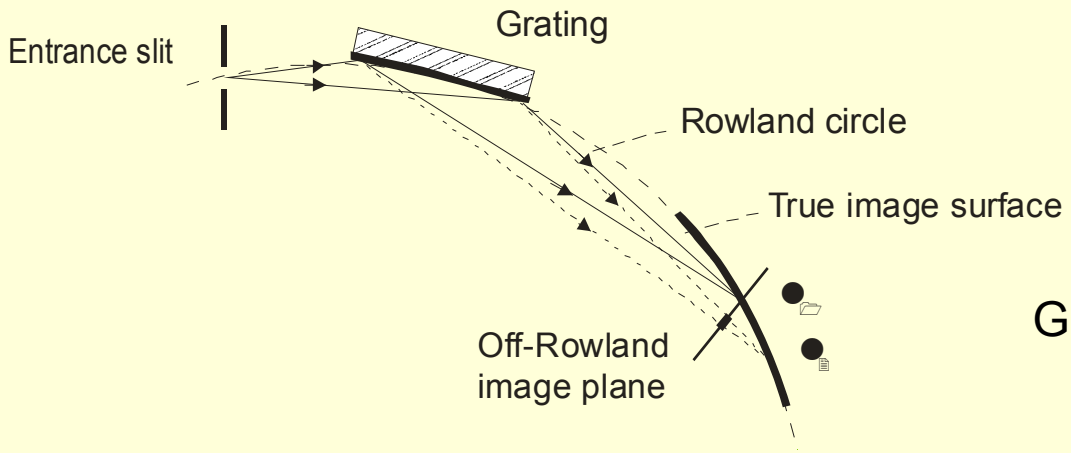

Grazing incidence mount
(high reflectivity)

Cylindrical concave grating
Spherical concave grating
Toroidal concave grating
Varying line spacing → flat field

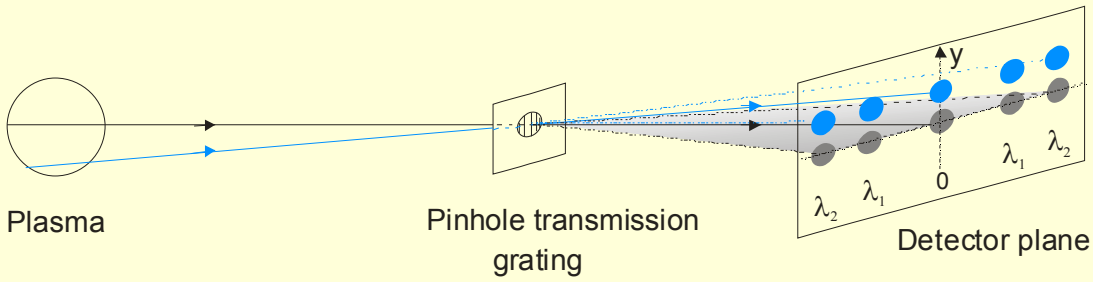

Pinhole
transmission grating

Introduction to Plasma Spectroscopy
H.-J. Kunze
Springer, Heidelberg, 2009